Protein Science (1995), *4*:2156-2167. Cambridge University Press. Printed in the USA.

The role of glutamate 87 in the kinetic mechanism of *Thermus thermophilus* isopropylmalate dehydrogenase

ANTONY M. DEAN AND LAURA DVORAK

Department of Biological Chemistry, The Chicago Medical School, N. Chicago, Illinois 60064-3095

(RECEIVED July 5, 1995; ACCEPTED August 7, 1995)

Abstract

The kinetic mechanism of the oxidative decarboxylation of 2R,3S-isopropylmalate by the NAD-dependent isopropylmalate dehydrogenase of *Thermus thermophilus* was investigated. Initial rate results typical of random or steady-state ordered sequential mechanisms are obtained for both the wild-type and two mutant enzymes (E87G and E87Q) regardless of whether natural or alternative substrates (2R-malate, 2R,3S-tartrate and/or NADP) are utilized. Initial rate data fail to converge on a rapid equilibrium-ordered pattern despite marked reductions in specificity (k_{cat}/K_m) caused by the mutations and alternative substrates. Although the inhibition studies alone might suggest an ordered kinetic mechanism with cofactor binding first, a detailed analysis reveals that the expected noncompetitive patterns appear uncompetitive because the dissociation constants from the ternary complexes are far smaller than those from the binary complexes. Equilibrium fluorescence studies both confirm the random binding of substrates and the kinetic estimates of the dissociation constants of the substrates from the binary complexes. The latter are not disturbed markedly by the mutations at site 87. Mutations at site 87 do not affect the dissociation constants from the binary complexes, but do greatly increase the Michaelis constants, indicating that E87 helps stabilize the Michaelis complex of the wild-type enzyme. The available structural data, the patterns of the kinetics results, and the structure of a pseudo-Michaelis complex of the homologous isocitrate dehydrogenase of *Escherichia coli* suggest that E87 interacts with the nicotinamide ring.

Keywords: IMDH; kinetic mechanism; stabilization of Michaelis complex

The isopropylmalate dehydrogenase (IMDH) from *Thermus thermophilus* (2R,3S-isopropylmalate:NAD^+ oxidoreductase [decarboxylating]; EC 1.1.1.85), the tartrate dehydrogenase (TDH) from *Pseudomonas putida*, and the isocitrate dehydrogenase (IDH) from *Escherichia coli* (2R,3S-isocitrate:$NADP^+$ oxidoreductase [decarboxylating]; EC 1.1.1.42) are homologous enzymes (Hurley et al., 1989; Imada et al., 1991; Tipton & Beecher, 1994) that catalyze dehydrogenations at the Cαs and decarboxylations at the Cβs of their respective 2-hydroxy acid substrates. The reactions occur in two steps, with dehydrogenation preceding decarboxylation, viz:

$$\text{2-Hydroxy acid} + \text{NAD(P)}^+ \xrightleftharpoons{Mg^{2+}} \text{2-Oxalo acid} + \text{NAD(P)H} + H^+$$

$$\text{2-Oxalo acid} + H^+ \xrightleftharpoons{Mg^{2+}} \text{2-Keto acid} + CO_2$$

The crystallographic structure of native *E. coli* IDH with bound 2R,3S-isocitrate (Hurley et al., 1991) is consistent with much previous work on the catalytic mechanism (Steinberger & Westheimer, 1951; Siebert et al., 1957; Lienhard & Rose, 1964; Londesborough & Dalziel, 1968; Erhlich & Colman, 1987; Grissom & Cleland, 1988), where the required magnesium, coordinated between the carboxylate and hydroxyl group of the Cα of 2R,3S-isocitrate, is in a position to stabilize negative charges formed on the hydroxyl oxygen during the transition states of both steps (Fig. 1A).

Despite sharing only 30% sequence identity, the crystallographic structure of apo IMDH reveals the same protein fold as IDH, one quite distinct from other dehydrogenases (Hurley et al., 1989; Imada et al., 1991). Although no crystallographic structures of IMDH with substrate bound are available, all amino acids in IDH and IMDH involved with binding and catalysis at the 2R-malate core common to their substrates are identical. Both enzymes catalyze hydride transfer onto the *re* faces of the nicotinamide rings of their cofactors (Kakinuma et al., 1989; Hurley et al., 1991). These observations suggest that the catalytic sites of IDH and IMDH are conserved.

The available crystallographic structures of IMDH (Imada et al., 1991; Hurley & Dean, 1994) are relatively open compared to the closed conformations seen with IDH. By structural analogy, then, closure is necessary to bring all residues involved with

Reprint requests to: Antony M. Dean, Department of Biological Chemistry, The Chicago Medical School, 3333 Green Bay Road, N. Chicago, Illinois 60064-3095; e-mail: deana@mis.finchcms.edu.

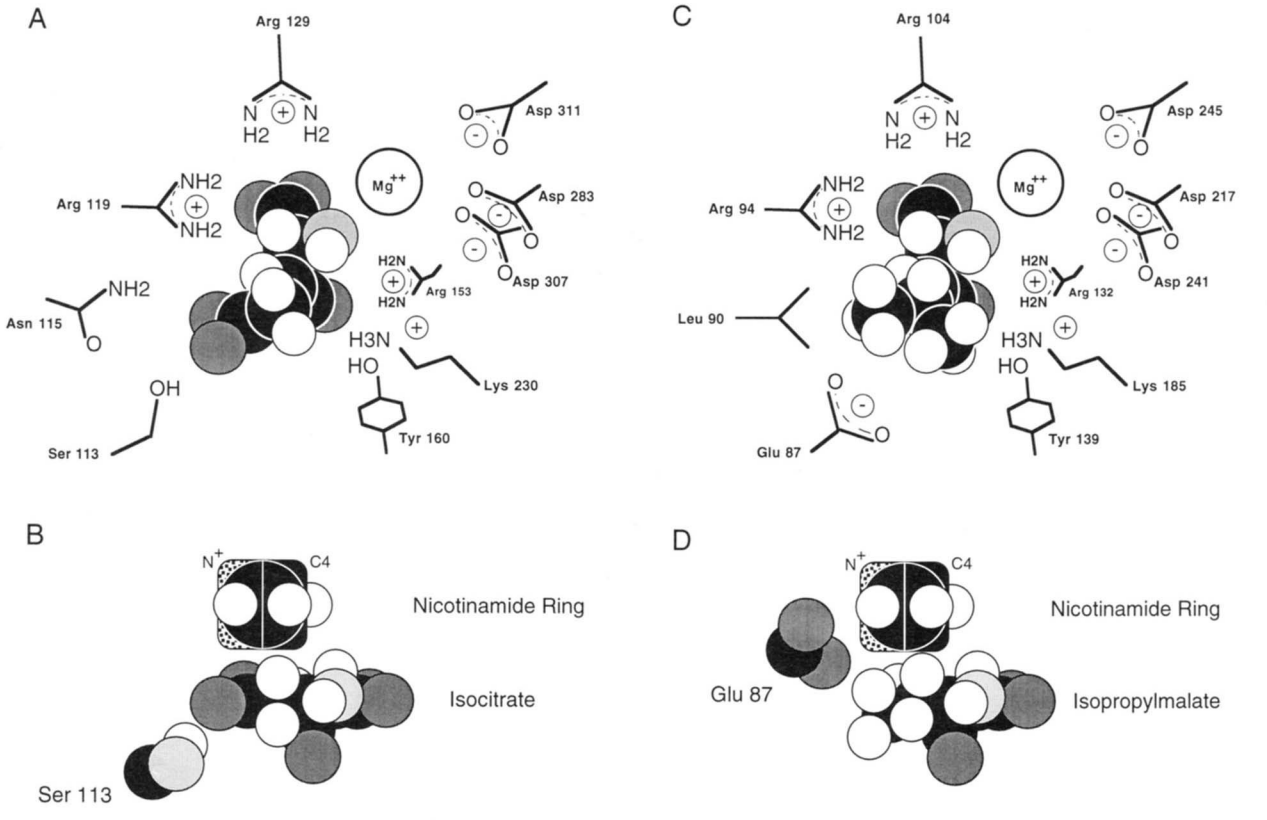

Fig. 1. A: Schematic diagram of the active site of IDH with bound 2R,3S-isocitrate. Spheres colored as follows: carbon, black; hydrogen, white; charged oxygens, heavy shading; uncharged oxygens, light shading. 2R,3S-isocitrate binds between the two domains of IDH in a pocket formed from both subunits. R119, R129, and R153 form hydrogen bonds to the α and β carboxylates of 2R,3S-isocitrate. The α-hydroxyl group and α-carboxylate of 2R,3S-isocitrate are chelated to a magnesium ion associated with D283 and D241 and two waters (not shown) in a roughly octahedral manner. The structure is consistent with much previous work on the catalytic mechanism, suggesting that dehydrogenation at the α-carbon precedes decarboxylation at the β-carbon. D283 of IDH is suitably aligned to act as a catalytic base abstracting a proton from the α-hydroxyl during dehydrogenation, and K230 probably acts as the catalytic acid donating a proton to the β-carbon during decarboxylation. The γ-carboxylate moiety of 2R,3S-isocitrate forms a hydrogen bond to the serine at site 113. **B:** In the pseudo-Michaelis complex of IDH, the γ-carboxylate of 2R,3S-isocitrate forms a salt bridge to the charged nitrogen of the nicotinamide ring, the C_4 of which is positioned to receive the α-carbon hydride of 2R,3S-isocitrate on the *re*-face. **C:** Proposed structure of the IMDH active site with 2R,3S-isopropylmalate bound. The active site of IMDH is clearly homologous to that of IDH, with three arginines (94, 104, and 132) available for hydrogen bonding to the carboxylates of 2R,3S-isopropylmalate, two aspartates (217 and 241) available for chelating magnesium, and a potentially catalytic lysine at position 185. The precise location of the side chain of E87 is not known, but it probably lies close to the γ-isopropyl moiety of the bound substrate, where it would be in a position to stabilize the nicotinamide ring for catalysis by forming a salt bridge to the charged nitrogen (**D**) or a hydrogen bond to the amide (not shown).

binding the 2R-malate moiety of the substrates together to form the 2R,3S-isopropylmalate binding site (Fig. 1C). A rigidly conserved glutamic acid at site 87 in IMDH occupies a position similar to S113 in IDH. Closure would inevitably bring this charged amino acid into the proximity of the hydrophobic γ-moiety of bound 2R,3S-isopropylmalate.

In the crystallographic structure of a pseudo-Michaelis complex of IDH, S113 hydrogen bonds to the γ-carboxylate of 2R,3S-isocitrate, which in turn, forms a salt bridge to the charged nitrogen of the nicotinamide ring (Fig. 1B), presumably stabilizing it in a position for catalysis (Stoddard et al., 1993). Indeed, in the absence of bound 2R,3S-isocitrate, the entire nicotinamide mononucleotide moiety of the cofactor is completely disordered (Hurley et al., 1991). Moreover, phosphorylation of S113 inactivates IDH by repelling the negative charge of the γ-carboxylate of the substrate, causing a marked increase in its dissociation constant, and disrupting alignment of the nicotinamide ring, causing a marked reduction in k_{cat} (Dean & Koshland, 1990; Hurley et al., 1990). These effects are mimicked when S113 is replaced by aspartate or glutamate (Dean et al., 1989; Dean & Koshland, 1990), both of which carry negatively charged side chains.

These observations suggest that E87 may help stabilize the IMDH Michaelis complex, much like the role played by the γ-carboxylate of bound 2R,3S-isocitrate in IDH (Fig. 1D), and at the same time may repel 2R,3S-isocitrate from the active site of IMDH, much like the phosphorylated serine in IDH. Indeed, the conformation of the cofactor in the IMDH binary complex, which is similar to that seen in the pseudo-Michaelis complex of IDH, brings the charged nitrogen of the nicotinamide ring within 4.4 Å of E87 (Hurley & Dean, 1994).

An understanding of the kinetic mechanism of IMDH is necessary prior to investigating the role of E87 in the active site of IMDH. All thoroughly investigated NADP-dependent IDHs cat-

alyze steady-state random mechanisms (eukaryotic mitochondria [Londesborough & Dalziel, 1970; Northrop & Cleland, 1974; Uhr et al., 1974]; the digestive gland of the mussel *Mytilus edulis* [Head, 1980]; and the prokaryote *E. coli* [Dean & Koshland, 1993]). By contrast, preliminary investigations suggest that TDH and IMDH catalyze ordered kinetic mechanisms with the cofactor binding first (Tipton & Peisach, 1991; Han & Pirrung, 1994).

Here, initial rate studies, alternative substrates, inhibition studies, and fluorescence equilibrium binding experiments with wild-type and mutant enzymes are used to elucidate the kinetic mechanism and investigate the role of E87 in the active site of IMDH.

Results

Enzyme purity

Following SDS-PAGE and staining with Coomassie blue, purified wild-type and mutant enzymes reveal the expected broad 35-kDa bands corresponding to IMDH. The preparations are substantially free of contaminating protein, although several minor bands are occasionally seen if more than 20 μg of protein are loaded per lane.

Alternative substrates

The substrate range of IMDH is broad (Miyazaki et al., 1993) so long as the 2R-malate core, which is essential for catalysis, is preserved. In addition to the published range (methyl-, ethyl-, isopropyl-, isobutyl-, tertbutyl-, and isoamyl moieties may be attached at the 3S-position of 2R-malate, which is also a substrate), IMDH can utilize 2R,3S-tartrate and NADP. Based on changes in absorbance at 340 nm, 2R,3S-isocitrate and 2R,2R-tartrate do not appear to be substrates (rates < 0.003/s at 50 mM substrate 5 mM NAD). However, this does not exclude the possibility that decarboxylation may occur in the absence of reduction of NAD as seen in TDH (Tipton & Peisach, 1991). 2S-malate and 2S,3S-tartrate do not appear to be substrates, a result consistent with the chirality of the active site.

Kinetic results

Michaelis constants in the submicromolar range were determined using 10-cm quartz cuvettes and, generally, rates remained linear for at least 200 s. Rates below 0.05 μM 2R,3S-isopropylmalate may be somewhat imprecise due to the inevitable curvature caused by consumption of the limiting substrate. Estimates of Michaelis constants exceeding 10 mM are probably biased due to difficulties in saturating the enzymes with substrates and associated changes in ionic strength and salt concentrations. Nevertheless, all estimates are reproducible within about 15% of the reported values.

Estimates of the kinetic parameters are presented in Tables 1 and 3. No evidence of substrate inhibition was detected. However, double reciprocal plots (Fig. 2) revealed evidence of weak cooperativity. The Hill coefficients are never greater than 1.15, and only in a few cases did partial regression analyses reveal that they make a significant contribution to a reduction in the residual sums of squares. In no case did omission of the Hill coefficients from the kinetic models significantly disturb estimates of V_{max} and K_m when analyses of the data are confined to substrate concentrations above the apparent Michaelis constants, where the weak nonlinearities are not so evident. Standard errors of the kinetic estimates are generally less than 15% of the estimates.

Initial rate studies

Initial rate studies (Table 1) were conducted using the natural substrate, 2R,3S-isopropylmalate, alternative substrates, 2R,3S-tartrate and 2R-malate, and both natural and alternative cofac-

Table 1. *Kinetic constants from initial rate studies*[a]

	Enzyme								
	E87			E87G			E87Q		
Substrate	K_i (μM)	K_m (μM)	k_{cat} (s^{-1})	K_i (μM)	K_m (μM)	k_{cat} (s^{-1})	K_i (μM)	K_m (μM)	k_{cat} (s^{-1})
IPM[b]	10.6	0.017	0.24	9.3	0.48	0.20	11.2	5.3	0.21
NAD	2,004	3.21		2,538	131		1,637	778	
IPM	7.75	2.98	1.66		ND[c]			ND	
NADP	4,782	1,836							
Tartrate	2,535	40.7	0.19	7,734	1,210	0.21	10,183	761	0.26
NAD	1,985	45.4		2,468	386		2,422	181	
Tartrate	2,918	817	0.10		ND			ND	
NADP	5,619	1,573							
Malate	30,923	1,510	10.59	35,590	35,590	0.26	32,600	32,600	0.19
NAD	2,182	106.5		2,584	2,584		1,853	1,853	
Malate	31,565	31,565	4.69		ND			ND	
NADP	6,579	6,579							

[a] Data were obtained in 25 mM MOPS, 100 mM KCl, 5 mM free Mg^{2+}, 1 mM dithiothreitol, pH 7.3 with KOH, at 21 °C.
[b] IPM, isopropylmalate.
[c] ND, not determined. All standard errors are less than 15% of the estimates.

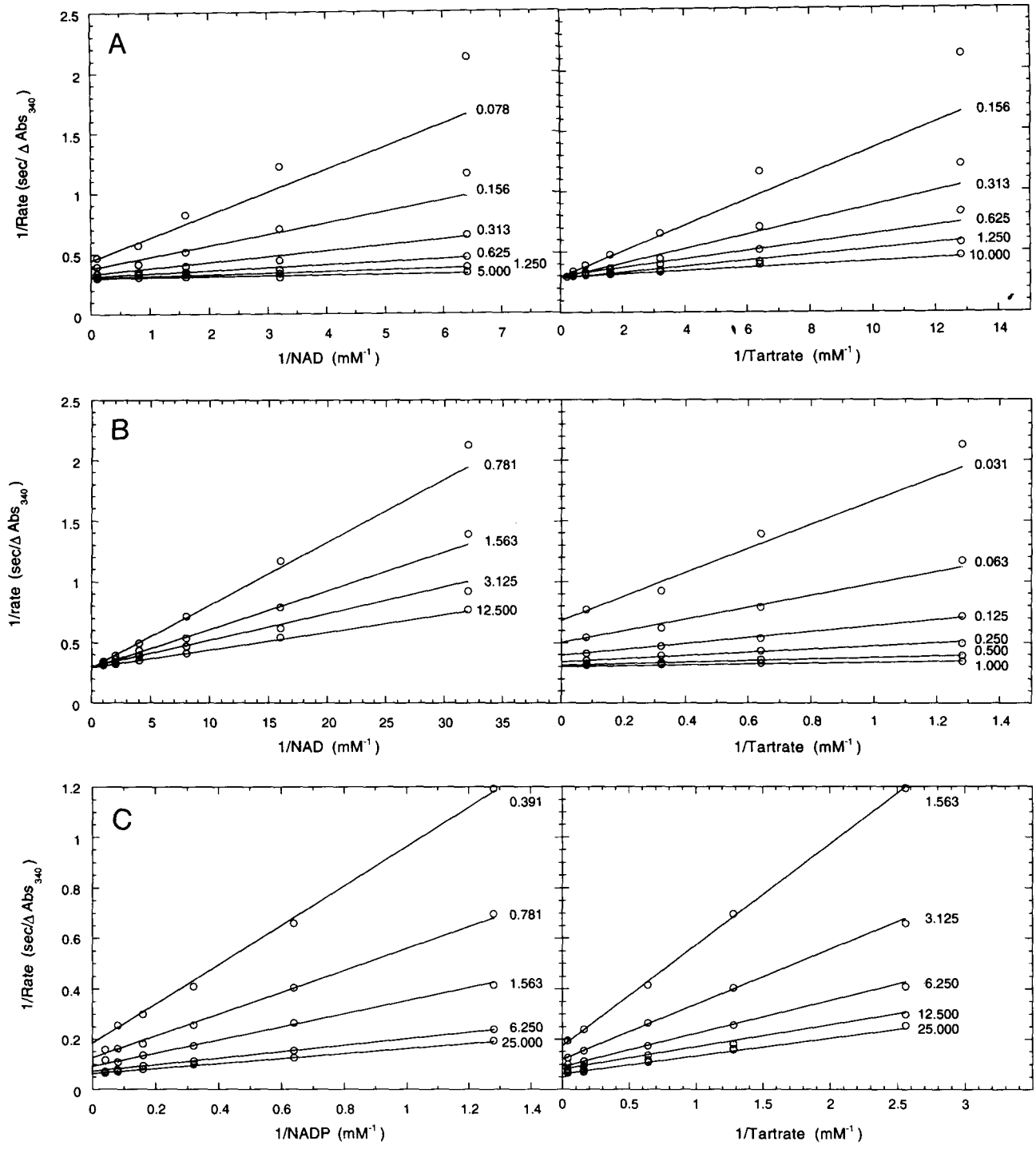

Fig. 2. Double reciprocal plots of data from three initial steady-state rate experiments for the oxidative decarboxylation of 2R,3S-tartrate by the wild-type E87 enzyme. **A:** Patterns suggest a rapid equilibrium-ordered mechanism with NAD binding first and 2R,3S-tartrate binding second. **B:** Patterns also suggest a rapid equilibrium-ordered mechanism, but this time with 2R,3S-tartrate binding first and NAD binding second. The apparent change in binding order was achieved merely by using different substrate concentrations. **C:** Results in the lower panels, where NADP is the cofactor, reveal linear intersecting patterns typical of random or steady-state ordered mechanisms. Lines describe the fits to Equation 1 using logarithmically transformed data.

tors (NAD and NADP). In all cases, Equation 1 provides an adequate fit to the data, suggesting that the sequential mechanism is either random or steady-state ordered. Note that using a limited range of substrate concentrations can generate double reciprocal plots typical of rapid equilibrium-ordered mechanisms, but by changing the range of substrate concentrations used the apparent order of binding is reversed (e.g., see Fig. 2). This situation arises whenever the dissociation constants from

the binary complexes are markedly larger than those from the Michaelis complexes. All reported kinetic estimates are determined from complete data sets encompassing the broad range of substrate concentrations.

The use of alternative substrates, cofactors, and mutant enzymes cause marked reductions in specificity (from k_{cat}/K_m = 1.4×10^7 M^{-1} s^{-1} with the wild-type enzyme utilizing 2R,3S-isopropylmalate to 6 M^{-1} s^{-1} for the E87Q mutant utilizing 2R-malate), yet never bring the mechanism sufficiently close to rapid equilibrium such that Equation 2 (rapid equilibrium ordered) provides an adequate fit to the data. Moreover, the dissociation constants for the substrates and cofactors from their binary complexes with each enzyme (the K_i's in Table 1) remain relatively unperturbed by the presence of alternative substrates and cofactor. Such are the hallmarks of a random kinetic mechanism (Huang, 1979).

Fluorescence studies

Addition of substrates (2R,3S-isopropylmalate, 2R,3S-tartrate, 2R-malate, or 2R,3S-isocitrate) to enzyme solutions do not produce detectable changes in the emission spectra between 300 and 500 nm when excited at 280 nm (Fig. 3A). Addition of NAD reduces peak fluorescence at 340 nm, but no more so than expected from inner filter effects. The addition of NADH also reduces peak fluorescence, the effect being more marked due to its absorbance at 340 nm. NADH also produces a peak at 450 nm that is indistinguishable from that obtained in the absence of enzyme. NAD and NADH spectra remain unaffected by the addition of substrates in the absence of enzyme.

The addition of substrate to a solution of enzyme containing a small quantity (20 μM) of NADH causes a marked decrease in fluorescence at 340 nm and a dramatic increase in fluorescence at 420 nm (Fig. 3A). This provides direct evidence for the formation of abortive E.NADH.substrate complexes, the fluorescent properties of which differ markedly from those of the free enzyme and the binary complexes with substrates or cofactors. The sole exception is the addition of 2R,3S-isocitrate, which does not generate any detectable increase at 420 nm (Fig. 3B). One possible explanation is that the γ-carboxylate of bound 2R,3S-isocitrate lies sufficiently close to the reduced nicotinamide ring to cause quenching. Nevertheless, the binding of 2R,3S-isocitrate can still be monitored by the drop in fluorescence at 340 nm in the presence of NADH (Fig. 3B) or NAD (not shown). These results provide direct evidence for the formation of abortive E.NAD(H).isocitrate complexes.

The weak cooperativity seen in the kinetics data is again evident in the binding of substrates, regardless of whether changes in emission are monitored at 340 or 420 nm (Fig. 4). Evidently, the cooperativity seen in the initial rate kinetics studies is caused by changing affinities, rather than changes in k_{cat}. The dissociation constants in Table 2 are calculated from data in the upper linear portions of the plots. The dissociation constants in Table 2 are based on changes in fluorescence at 420 nm, which avoids the strong absorbance of NADH at 340 nm when the latter is the varied ligand.

Figure 5A illustrates results from a fluorescence experiment with the wild-type enzyme in which 2R,3S-isopropylmalate is varied at fixed concentrations of NADH. The straight line, representing the expected relation for an ordered mechanism in which 2R,3S-isopropylmalate binds second, is clearly at variance

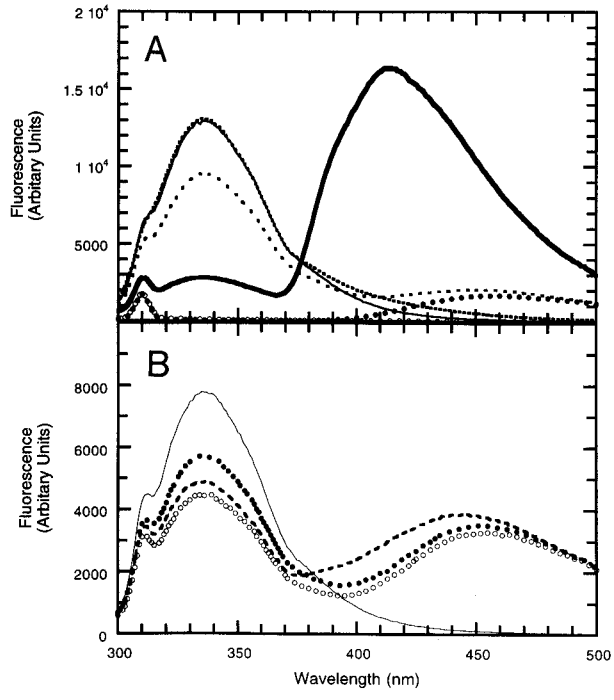

Fig. 3. Fluorescence spectra (excitation at 280 nm) of the wild-type E87 (**A**) and mutant E87G (**B**) enzymes. **A:** Buffer with 2R,3S-isopropylmalate (○○○○) or with 10 μM NADH (●●●●); wild-type E87 enzyme alone (——); 10 μM NADH reduces apparent protein fluorescence at 340 nm by absorbing at 280 nm and 340 nm (■■■■); 50 μM 2R,3S-isopropylmalate has little effect on protein fluorescence (▪▪▪▪▪▪) unless NADH is present (▬▬), in which case a dramatic drop in fluorescence at 340 nm occurs and a new peak at 420 nm appears. **B:** Mutant E87G enzyme with 15 mM 2R,3S-isocitrate (———) or 20 μM NADH (●●●●) present; addition of 5 mM 2R,3S-isocitrate in the presence of 20 μM NADH (○○○○) causes a drop in fluorescence at 340 nm, but does little to change fluorescence at around 450 nm; as with the wild-type enzyme, addition of 10 μM 2R,3S-isopropylmalate in the presence of 20 μM NADH causes a drop in fluorescence at 340 nm and a marked shift in fluorescence at 450 nm (·····); further addition of 5 mM 2R,3S-isocitrate has little effect on fluorescence at 340 nm, but the peak at 450 nm drops (▬ ▬ ▬), a consequence, perhaps, of competitive binding.

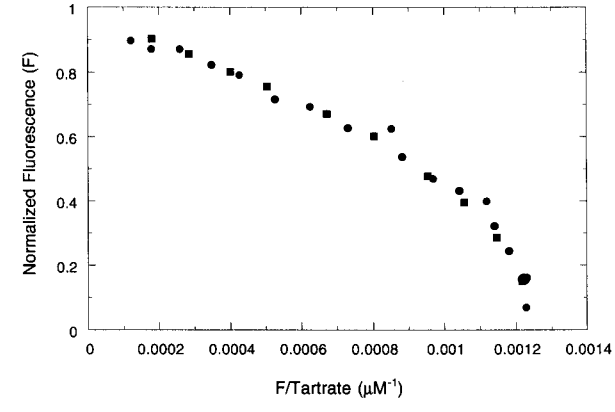

Fig. 4. An Eadie–Hoftsee plot of the equilibrium binding of 2R,3S-tartrate to the wild-type enzyme in the presence of 50 μM NADH monitored by fluorescence at 340 nm (●) and 420 nm (■). The weak positive cooperativity (the Hill coefficient = 1.13 ± 0.04 is typical for all substrates) is similar to that detected in the kinetics experiments. Estimates of the dissociation constants were calculated using data above $F = 0.5$, where the effects of cooperativity are no longer evident.

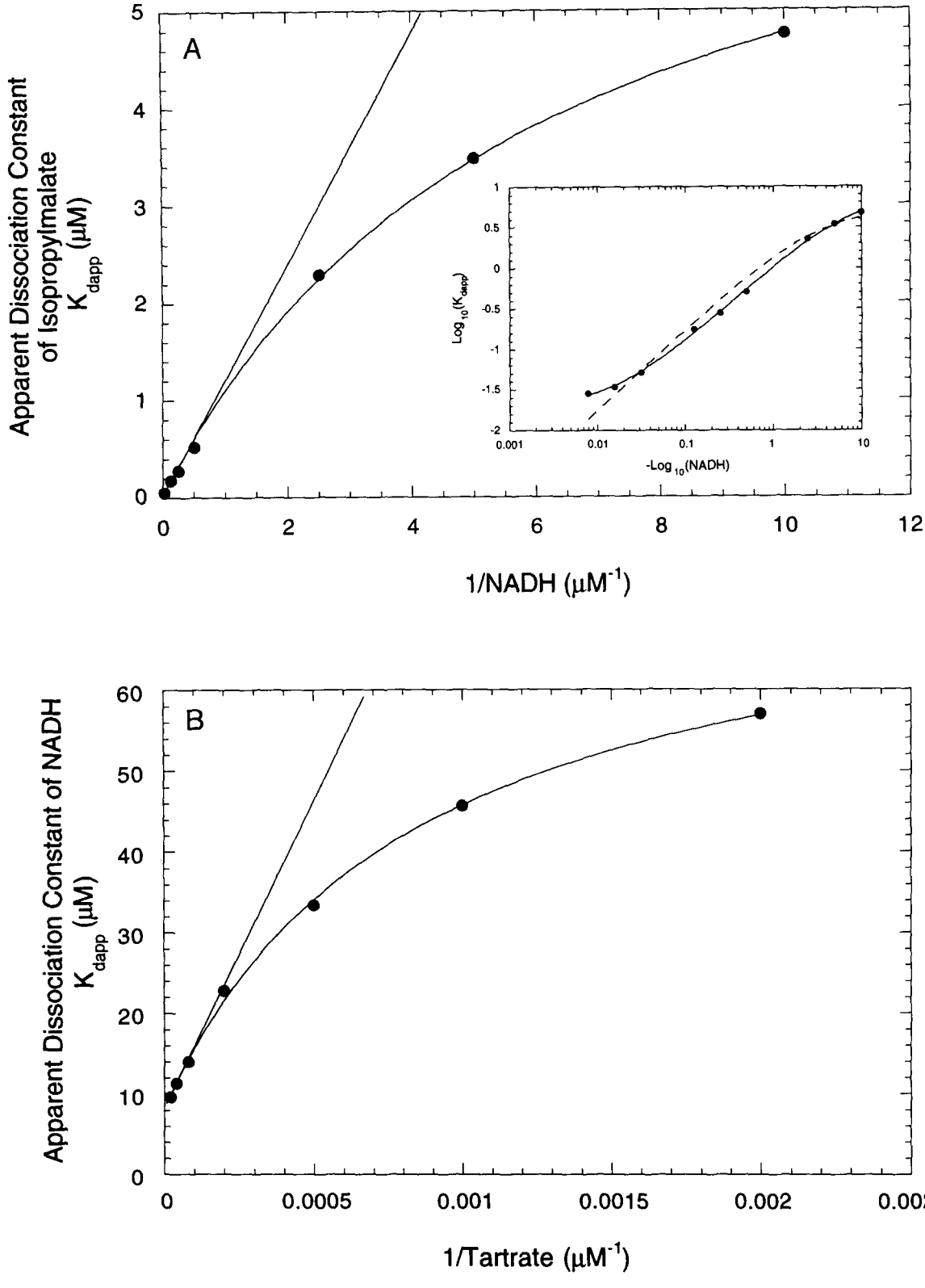

Fig. 5. Secondary plots of the apparent dissociation constants of varied substrates (obtained from fluorescence experiments such as those in Fig. 4) as functions of the reciprocal of the concentration of the fixed substrates. In both plots, the straight lines represent the expected relations if the fixed substrate binds first (Equation 8) and the curves are fits to random binding (Equation 7) using logarithmically transformed data. **A:** Equilibrium binding of 2R,3S-isopropylmalate to the wild-type E87 enzyme at fixed concentrations of NADH. The inset shows the same data on a log-log scale with fit to the random model of Equation 7 (———) tracking the data better than the fit to the ordered model (Equation 9) with the fixed substrate binding second (– – – –). **B:** Equilibrium binding of NADH to the mutant E87G enzyme at fixed concentrations of 2R,3S-tartrate.

Table 2. *Equilibrium binding constants from fluorescence studies*[a]

	Enzyme					
	E87		E87G		E87Q	
Substrate	K_i^f (μM)	K_m^f (μM)	K_i^f (μM)	K_m^f (μM)	K_i^f (μM)	K_m^f (μM)
IPM[b]	8.4	0.018	11.1	0.4	14.3	5.1
NADH	65.5	0.14	59	1.6	70	25
Tartrate	2,766	161	11,360	1,210	5,860	1,220
NADH	122	7.1	77	8.2	120	25
Malate	37,135	1,605	28,400[c]	29,600[d]	23,870[c]	26,750[d]
NADH	118	5.1	ND[e]	ND	ND	ND
Isocitrate	ND	173.4	261	9.4	153	9.8
NAD	2,492	ND	2,123	76.5	1,746	112

[a] Data were obtained in 25 mM MOPS, 100 mM KCl, 5 mM free Mg^{2+}, 1 mM dithiothreitol, pH 7.3 with KOH, at 21 °C.
[b] IPM, isopropylmalate.
[c] Determined at 10 mM NADH.
[d] Determined at 400 mM NADH.
[e] ND, not determined. All standard errors are less than 15% of the estimates.

with the data. Equation 8, which describes the binding 2R,3S-isopropylmalate first and then NADH, provides an acceptable fit to the untransformed 2R,3S-isopropylmalate data. However, when Equation 8 is fitted to logarithmically transformed data, the curve systematically underestimates the apparent dissociation constants of 2R,3S-isopropylmalate at high concentrations of NADH. Equation 7, which describes random binding, provides a much better fit with the curve tracking the data properly and intercepting the Y-axis above the origin (Fig. 5A, inset). Hence, the data support random binding of 2R,3S-isopropylmalate and NADH, a result consonant with the conclusions from the initial rate studies.

Figure 5B illustrates results from an experiment with the E87G mutant, where NADH is varied at fixed concentrations of 2R,3S-tartrate. The fact that the fitted curve is not linear (as in Equation 9) and does not pass through the origin (as in Equation 8 when B is saturating) supports a random mechanism (data fitted to Equation 7). The binding of 2R,3S-isopropylmalate to the E87Q mutant produces similar results.

The results from the fluorescence equilibrium binding studies (Table 2) support random binding, in agreement with the results from the initial rate studies with alternative substrates. Indeed, the estimated K_i^f's for the substrates and cofactors calculated using Equation 7 are in agreement with the K_i's obtained from the initial rate studies (Table 1). Moreover, the equilibrium fluorescence binding studies provide direct evidence for E.NADH.substrate abortive complexes and the E.NAD.isocitrate dead end complexes (Fig. 6).

Inhibition studies

NADH always produces competitive inhibition patterns with respect to NAD and noncompetitive inhibition patterns with respect to the substrates (Table 3). Although these observations are consistent with Figure 6, an ordered steady-state mechanism with cofactor binding first can produce similar inhibition patterns.

2R,3S-tartrate, by virtue of its low k_{cat}, can be used as an effective inhibitor of the wild-type enzyme, catalyzing the reaction with 2R-malate. As expected, 2R,3S-tartrate produces competitive inhibition patterns with respect to this substrate. The K_i = 50 μM of 2R,3S-tartrate obtained at 20 mM NAD (Table 3) when 2R-malate is utilized as a substrate is similar to the K_m = 40.7 μM of 2R,3S-tartrate when it is the substrate (Table 1). Such equivalence is expected for a rapid equilibrium random mechanism, but not for a steady-state ordered mechanism.

Interestingly, 2R,3S-tartrate produces uncompetitive patterns with respect to NAD. Similar patterns were obtained with 2R,3S-isocitrate as an inhibitor, regardless of substrate or mutant enzyme used (Table 3). Such results are usually taken as diagnostic of an ordered kinetic mechanism with cofactor binding first. However, any inhibitor having a high affinity for the

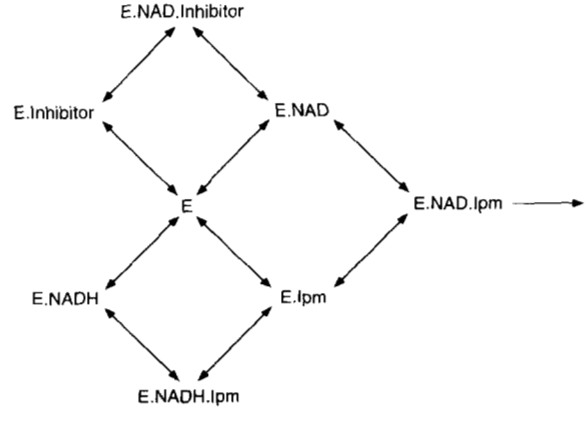

Scheme I

Fig. 6. IMDH from *T. thermophilus* catalyzes a random kinetic mechanism in the direction of oxidative decarboxylation of the 2-hydroxy acid substrates. Two abortive complexes form, E.NADH.substrate and E.NAD.inhibitor.

Table 3. *Kinetic constants from inhibition studies*[a]

Enzyme	Varied substrate	Inhibitor	Pattern[b]	K_{is} (mM)	K_{ii} (mM)	Fixed substrate	Concentrations (μM)
E87	IPM[c]	Isocitrate	C	617 ± 150		NAD	2,000
	NAD	NADH	C	0.111 ± 0.004		IPM	12
	Malate	Isocitrate	C	237 ± 2		NAD	20,000
	Malate	Tartrate	C	50 ± 4		NAD	20,000
	Malate	Tartrate	C	72 ± 5		NAD	2,000
	Malate	NADH	NC	400 ± 70	389 ± 23	NAD	2,000
	NAD	Isocitrate	UC		321 ±12	Malate	1,000
	NAD	Tartrate	UC		164 ± 3	Malate	1,000
	NAD	NADH	C	192 ± 19		Malate	1,000
	Tartrate	Isocitrate	C	246 ± 43		NAD	20,000
	Tartrate	NADH	NC	528 ± 68	669 ± 29	NAD	2,000
	NAD	Isocitrate	UC		567 ± 42	Tartrate	100
	NAD	Isocitrate	UC		680 ± 16	Tartrate	125
	NAD	Isocitrate	UC		4,478 ± 210	Tartrate	1,000
	NAD	NADH	C	152 ± 18		Tartrate	150
E87Q	IPM	Isocitrate	C	20 ± 2		NAD	2,000
	IPM	NADH	NC	36 ± 4	73 ± 4	NAD	2,000
	NAD	Isocitrate	UC		48 ± 2	IPM	50
	NAD	NADH	C	16 ± 1		IPM	20
	Malate	Isocitrate	C	32 ± 4		NAD	750
	Malate	NADH	NC	75 ± 3	139 ± 13	NAD	750
	NAD	Isocitrate	UC		29 ± 1	Malate	25,000
	NAD	NADH	C	84 ± 5		Malate	25,000
	Tartrate	Isocitrate	C	23 ± 3		NAD	1,250
	Tartrate	NADH	NC	139 ± 15	194 ± 9	NAD	1,250
	NAD	Isocitrate	UC		15 ± 1	Tartrate	1,250
	NAD	NADH	C	61 ± 3		Tartrate	1,250
E87G	Tartrate	Isocitrate	C	24 ± 3		NAD	5,000
	Tartrate	NADH	NC	172 ± 19	79 ± 2	NAD	3,000
	NAD	Isocitrate	UC		29 ± 2	Tartrate	1,000
	NAD	Isocitrate	UC		69 ± 2	Tartrate	5,000
	NAD	NADH	C	50 ± 3		Tartrate	2,500
	NAD	NADH	C	48 ± 4		Tartrate	250

[a] Data were obtained in 25 mM MOPS, 100 mM KCl, 5 mM free Mg^{2+}, 1 mM dithiothreitol, pH 7.3 with KOH, at 21 °C.
[b] C, competitive inhibition; NC, noncompetitive inhibition; UC, uncompetitive inhibition.
[c] IPM, isopropylmalate.

E.NAD binary complex relative to the free enzyme can force the noncompetitive pattern expected of a random kinetic mechanism with a dead-end complex to appear uncompetitive. This is a particular concern here because 2R,3S-tartrate and 2R,3S-isocitrate (Table 2) have much higher affinities for the E.NAD binary complexes than the free wild-type enzyme (Table 1). Indeed, when the kinetic constants in Table 1 and the equilibrium binding constants in Table 2 are inserted into the equation describing noncompetitive inhibition for a random kinetic mechanism, namely

$$v = \frac{\dfrac{VAB}{(K_{mA} + A)}}{\left[K_{iB} \cdot \dfrac{(1 + A/K_{iA})}{(1 + A/K_{mA})} \cdot \left(1 + \dfrac{I}{K_{is}(1 + A/K_{iA})}\right) + B \cdot \left(1 + \dfrac{I}{K_{ii}(1 + A/K_{mA})}\right)\right]},$$

the simulated results show that isocitrate (I) generates the appearance of uncompetitive patterns with respect to NAD (B), regardless of the concentrations of fixed substrate (A) when the latter is unsaturating.

If the patterns generated from these inhibition studies do not provide a means to distinguish between random and ordered mechanisms, the initial rate studies with alternative substrates and fluorescence equilibrium binding studies provide unambiguous evidence supporting a random mechanism with the formation of abortive and dead-end complexes (Fig. 6).

Discussion

The kinetic mechanism

Initial rate studies, utilizing both natural and alternative substrates and cofactors, inhibition studies, and equilibrium binding studies of wild-type and mutant enzymes, demonstrate that the IMDH from *T. thermophilus* catalyzes a random kinetic

mechanism in the direction of oxidative decarboxylation of the 2-hydroxy acid substrates, and that two abortive complexes, E.NADH.substrate and E.NAD.inhibitor, form (Fig. 6). Reports suggesting that IMDH catalyzes an ordered mechanism should be treated with caution given such wide separations between K_i's and K_m's, which can cause initial rate data to appear characteristic of rapid equilibrium ordered mechanisms (Fig. 2) and noncompetitive inhibition patterns to converge on uncompetitive ones (Table 3).

A proposed role for the conserved E87

A detailed understanding of the role played by the conserved E87 ultimately requires determination of the crystallographic structure of an IMDH ternary complex. Unfortunately, no structures of IMDH with bound substrate/inhibitors are available. However, the striking homologies between the catalytic sites of IMDH and IDH (Fig. 1A,C) suggest that the nicotinamide ring in the IMDH Michaelis complex may adopt a position similar to that in the IDH pseudo-Michaelis complex, lying above the γ-isopropyl moiety, with E87 stabilizing it in that position in a manner reminiscent of the role played by the γ-carboxylate of 2R,3S-isocitrate in IDH (Fig. 1B,D).

Such an arrangement might be taken as evidence for an ordered kinetic mechanism with the substrate binding first, because the nicotinamide ring of the bound cofactor might be expected to block access to the active site. However, the crystallographic structure of IMDH with bound NAD has been determined (Hurley & Dean, 1994) and reveals that the nicotinamide ring is only partially ordered and that further closure of the two domains is necessary to form the substrate binding site. Evidently, the conformation of NAD in its binary complex does not block the active site, which remains accessible to substrate. Hence, the available crystallographic results are consistent with the proposed random mechanism.

The role of E87 in the binary complexes

In the binary complex of IMDH with NAD, E87 lies 4.4 Å from the charged nitrogen of the nicotinamide ring (Hurley & Dean, 1994). Although electrostatic interactions can readily occur across such distances, the presence of water, its high dielectric constant, together with the observation that the nicotinamide ring is only partially ordered, suggests that any interaction should be weak. As expected, neither mutant at site 87 greatly affects the K_i's of the cofactors (Tables 1, 2).

Nor do the mutations greatly affect the K_i's of 2R,3S-isopropylmalate and 2R-malate (Tables 1, 2). That E87 plays no role in stabilizing the closed conformation of IMDH necessary for formation of the substrate binding site is also suggested by the available structural data. Direct interactions between E87 and the γ-moieties of these substrates seem unlikely, as do interactions with adjacent amino acids (P86 and L90).

That E87 plays no role in stabilizing the binary complexes is also consistent with the notion that E87 lies outside the active site. Yet equilibrium binding experiments with 2R,3S-isocitrate suggest otherwise. Fluorescence studies show that 2R,3S-isocitrate forms binary complexes with the mutant enzymes, but not with the wild-type enzyme (Table 2). This suggests that residues at site 87 lie close to the γ-moiety of bound 2R,3S-isocitrate, and that the mutations eliminate an inevitable electrostatic repulsion, thereby improving binding. Interestingly, E87 may also interact weakly with the 3S-hydroxyl of bound 2R,3S-tartrate because the mutants also reduce the stabilities of the binary complexes with this substrate (Tables 1, 2).

The role of E87 in the ternary complexes

If E87 lies close to the γ-moieties of the bound ligands in the ternary complexes, then replacing it with an uncharged amino acid should also eliminate the inevitable electrostatic repulsion with the γ-carboxylate of bound 2R,3S-isocitrate. Indeed, the K_m's of the mutant enzymes toward 2R,3S-isocitrate are reduced by a factor of 18 compared to the wild-type enzyme (Table 2). This becomes all the more impressive when compared to K_m's with 2R,3S-isopropylmalate, which are increased by factors between 30 and 300 (similar results are obtained with 2R-malate and 2R,3S-tartrate, Tables 1, 2), yielding overall changes in affinity between 540 and 5400.

In analogy with IDH, the most plausible mechanism by which E87 stabilizes the Michaelis complex remains a direct interaction with the cofactor, trapping ligands between the nicotinamide ring and the protein. This might be achieved by a hydrogen bond to the amide or a salt bridge to the charged nitrogen, both on the nicotinamide ring, or a hydrogen bond to the attached ribose.

The role of E87 in catalysis

2R-malate produces a very low k_{cat} with IDH (Dean & Koshland, 1990). Low k_{cat}'s (between 10^{-4} and 5×10^{-4}-fold lower than that with 2R,3S-isocitrate) are also obtained with the homologous series -CH_3, -CH_2CH_3, -$CH_2CH_2CH_3$, -CH_2CHCH_2, -CH_2CH_2OH, and -CH_2CHO attached at the 3S position of 2R-malate (A.M. Dean, A.K. Shiau, & D.E. Koshland Jr., unpubl. data). These observations are consistent with the notion that the negative charge of the γ-moiety of 2R,3S-isocitrate is crucial for alignment of the nicotinamide ring for efficient catalysis in IDH. In contrast, the k_{cat}'s of wild-type IMDH toward 2R,3S-tartrate and 2R,3S-isopropylmalate are similar (Table 1). Furthermore, Miyazaki et al. (1993) report that the k_{cat}'s for wild-type IMDH operating at 60° are quite similar for methyl-, ethyl-, and isopropyl- γ-moieties attached to 2R-malate. These observations demonstrate that the γ-isopropyl moiety plays no direct role in catalysis by IMDH, and that the enzyme itself must align the nicotinamide ring.

Substitutions for E87 reduce k_{cat} by a factor of 50 with 2R-malate, lending credence to the notion that this residue can play a role in aligning the nicotinamide ring for catalysis. However, these same mutants have no discernible effect on k_{cat} when either 2R,3S-isopropylmalate or 2R,3S-tartrate is the substrate. Inspection of Table 1 reveals that the k_{cat} of wild-type IMDH toward 2R-malate is aberrantly high. Precisely why elimination of the negatively charged glutamate has so little effect on k_{cat} of substrates with γ-moieties attached at the 3S position is not known, but a very tentative explanation can be proposed.

Whereas the nicotinamide mononucleotide moiety of the cofactor is stabilized by a single negatively charged moiety on the bound substrate in IDH, it is stabilized by two negatively charged amino acids in IMDH (D78 and E87). In IDH, elimination of the negative charge inevitably reduces k_{cat}. But in IMDH, elimination of the negative charge of E87 need not cause

a reduction in k_{cat} if the bifurcating hydrogen bond between D78 and the ribose hydroxyls is still sufficient to align the C4 of the nicotinamide ring for catalysis. This suggestion is all the more reasonable because of the limited degrees of freedom associated with the nicotinamide ribose moiety, particularly because a bifurcating hydrogen bond may also stabilize the sugar pucker.

Conclusion

The oxidative decarboxylation of 2-hydroxy acid substrates by the IMDH of *T. thermophilus* occurs via a random kinetic mechanism with the formation of two abortive complexes, E.NADH.substrate and E.NAD.inhibitor (Fig. 6). The available X-ray structures and kinetic data for the wild-type and site-directed mutant enzymes suggest that E87 interacts directly with the nicotinamide ring only in the Michaelis complex, and that this interaction, together with hydrogen bonds from D87 to the nicotinamide ribose hydroxyls, helps stabilizes the Michaelis complex.

Materials and methods

Growth conditions and strains

E. coli strain C600 (which is *LeuB*$^-$) was routinely grown at 37 °C in Luria broth (10 g bactotryptone, 5 g yeast extract, 10 g NaCl in 1 L with 15 g of bactoagar added for plates). Transformants were selected in the presence of 50 μg/mL of ampicillin.

Molecular biology

All gene manipulations were conducted using standard methods (Sambrook et al., 1989) and procedures recommended by the manufactures of the molecular biology products used.

Plasmid pUTL119 (Kagawa et al., 1984), which carries the *T. thermophilus* HB8 *LeuB* gene encoding IMDH, was transformed into *E. coli* C600. pUTL119 was purified, digested with *Bam*H 1, and a resulting 1.2-kb fragment electroeluted from an agarose gel, precipitated and lyophilized. Plasmid pEMBL18 (−) was similarly digested with *Bam*H 1 and the enzyme heat inactivated at 70 °C for 1 h. The 1.2-kb fragment was ligated into the digested plasmid with T4 DNA ligase. Following transformation into strain C600, plasmids carrying the 1.2-kb insert were identified by electrophoresis of *Bam*H 1 digests. The orientations of the inserts were determined by the dideoxy sequencing method (Sanger et al., 1977). A plasmid, pLD1, was identified with the *LeuB* gene in the correct orientation for protein expression from the *lac* promotor of the pEMBL18 (−) vector.

The uridine-labeled template method of Kunkel (1985) was used to replace the glutamate at site 87 in the *LeuB* gene of pLD1 with a glutamine and a glycine. Single-stranded uridine-labeled template was prepared using strain CJ236 and helper phage R401. Oligomer primers containing the necessary mismatches were synthesized using a Biosearch 8700 DNA Synthesizer. The mutants were identified by sequencing, and again confirmed by sequencing.

Growth and disruption of cells

E. coli strain C600, harboring a plasmid encoding either the wild-type *LeuB* gene or a site-directed mutant, was grown to full density in 6 L of Luria broth and harvested by centrifugation. Sixty milliliters of ice cold extract buffer (10 mM KH_2PO_4, 0.5 M KCl, 2 mM $MgCl_2$, 0.03% 2-mercaptoethanol, pH 7.7 with KOH) were added to 20 g of cell paste and sonicated for 30 s every 3 min for a total of 10 bursts.

Protein purification

Isopropylmalate dehydrogenase was purified using, with some modifications, the method of Yamada et al. (1990). Two milliliters of extract buffer containing 60 mg of protamine sulfate were added dropwise to the sample, stirred on ice for 30 min, and the pellet removed by centrifugation. The supernatant was heated for 20 min at 75 °C and the precipitated proteins removed by centrifugation. This step was again repeated, and the resulting supernatant subjected to ammonium sulfate fractionation. The pellet formed between 15% and 55% saturation at 4 °C was resuspended in 12 mM K_2HPO_4, 4 mM citric acid, 10 mM $MgCl_2$, 0.05% trichloromethylpropanol, 0.1% 2-mercaptoethanol, pH 6.2, and dialyzed against the same. The protein solution was applied to an ion exchange column of DEAE sephacel, and eluted with a linear gradient of 0–200 mM KCl. Fractions containing peak activities, and that correlate with the peak bands on SDS-PAGE gels, were pooled and dialyzed overnight against storage buffer (0.9 mM citric acid, 3.5 mM K_2HPO_4, 100 mM KCl, 2 mM dithiothreitol, 0.02% NaN_3, pH 6.2), concentrated using Centricon 50 molecular sieves, and frozen in liquid nitrogen. SDS-PAGE followed by staining with Coomassie blue was used to determine the purity of the preparations. Protein concentrations were determined using a molar extinction coefficient of 30,420 ΔA_{280nm}/cm (Kagawa et al., 1984).

Kinetics assays

The kinetic parameters of IMDH were determined in an assay buffer of 25 mM MOPS, 100 mM KCl, 1 mM dithiothreitol, pH 7.3 with KOH, at 21 °C in the presence of 5 mM free Mg^{2+}. The quantity of $MgCl_2$ necessary was determined using estimates of the Mg^{2+}-substrate and Mg^{2+}-coenzyme dissociation constants determined by Dean and Koshland (1993). The dissociation constants of 2R,3S-isopropylmalate are sufficiently low that the reductions in free Mg^{2+} concentrations are negligible even when enzymes are fully saturated. Consequently, the pK_d for 2R,3S-isopropylmalate was not determined and the experiments conducted at 5 mM $MgCl_2$. All dissociation constants are presented in terms of total substrate present (i.e., [Substrate] + [Mg^{2+}.Substrate]). The rates of reaction were determined by monitoring the production or consumption of NAD(P)H at 340 nm in a 1-cm light path using a Hewlett-Packard 8452A single-beam diode array spectrophotometer with internal referencing at 540 nm. The concentration of NAD(P)H was determined using a molar extinction coefficient of 6,200 ΔA_{340nm}/cm. Ten-centimeter quartz cuvettes were required to determine Michaelis constants, which were submicromolar, the enzyme concentrations never exceeding 10 pM. For initial rate studies, the concentration of one substrate was varied at several fixed levels of the second substrate.

Fluorimetry

Fluorescence studies were conducted in the same assay buffer used for the kinetic studies. Data were collected on a SLM 8100

spectrofluorometer equipped with two MC200 monochrometers and a thermostatted cell holder. One-centimeter quartz cuvettes were used when the concentrations of NAD or NADH were held constant. Four-millimeter quartz cuvettes were used to help minimize inner filter effects when NADH was the variable ligand. In both cases, slit widths were set at 4 mm. Excitation at 280 nm enabled changes in peaks at 340 nm, 420 nm, and 450 nm to be monitored simultaneously. The fixed concentration of enzyme used was typically around 150 nM, except where the dissociation constants were below 1 μM and where the fixed concentrations were reduced to around 10 nm. A positive displacement pipette was used to add small quantities of high concentrations of the varied ligand, the final volume at the end of each experiment never exceeding the sample volume (2 mL) by more than 5%.

Data analyses

Unweighted nonlinear least-squares Newton-Raphson regressions were used to determine the fit of complete kinetics data sets to the following models. Following the notation of Cleland (1963):

$$v = VAB/(K_{ia}K_b + K_aB + K_bA + AB)$$

Sequential Bi (Random or steady-state ordered), (1)

where A and B are the substrate concentrations, v is the velocity, V is the maximum velocity, K_{ia} is the apparent dissociation constant of the $E.A$ binary complex ($E.A \leftrightarrow E + A$), and K_a and K_b are the Michaelis constants for A and B from the $E.A.B$ ternary complex. For a rapid equilibrium-ordered kinetic mechanism, Equation 1 becomes:

$$v = VAB/(K_{ia}K_b + K_bA + AB)$$

Rapid equilibrium ordered Bi (2)

The equations describing the effects of an inhibitor I are:

$$v = VA/(K(1 + I/K_{is}) + A)$$

Linear competitive inhibition (3)

$$v = VA/(K + A(1 + I/K_{ii}))$$

Linear uncompetitive inhibition (4)

$$v = VA/(K(1 + I/K_{is}) + A(1 + I/K_{ii}))$$

Linear noncompetitive inhibition (5)

where K is the apparent Michaelis constant of the substrate whose concentration is varied, and K_{is} and K_{ii} are the slope and intercept inhibition constants (Cleland, 1963). There is a complementary set of equations describing the effects of the inhibitor when the concentration of B is varied and the concentration of A is fixed. Finally, logarithmic transformations of the data were used for fitting whenever K_i's were separated from K_m's by factors exceeding 10.

Unweighted nonlinear least-squares Newton-Raphson regressions were used to determine the fit of individual fluorescence data sets to the following Michaelian model:

$$F = F_{max}A/(K^f_{dapp} + A), \quad (6)$$

where F is the observed fluorescence, F_{max} and K^f_{dapp} are the apparent maximum fluorescence and dissociation constant at a fixed concentration of substrate, and A is the concentration of the varied substrate. Two corrections for F were necessary when NADH was the varied ligand. First, the fluorescence of NADH at 420 nm was determined and subtracted from that in the presence of fixed ligand. Second, the absorbance of NADH at 280 nm generates an inner filter effect that was corrected using the calculation of Brand and Witholt (1967).

Estimates of the dissociation and Michaelis constants were determined using unweighted nonlinear least-squares Newton-Raphson regressions to the following models:

$$K^f_{dapp} = K^f_a/(K^f_{ib} + B)/(K^f_b + B) \quad \text{Random, } A \text{ varied,} \quad (7)$$

$$K^f_{dapp} = K^f_{ia}K^f_b/(K^f_b + B) \quad \text{Ordered, } A \text{ varied,} \quad (8)$$

$$K^f_{dapp} = K^f_b(K^f_{ia}/A + 1) \quad \text{Ordered, } B \text{ varied.} \quad (9)$$

Although this approach avoids fitting data to complete models, it eliminates errors due to different concentrations of enzyme used from experiment to experiment and complications due to inner filter effects arising from the high concentrations of cofactors necessary in many experiments. Where practical, however, F_{max} (after a correction for inner filter effects) was fitted to an equation similar in form to Equation 6, thereby providing a check on the estimate of K^f_b. Again, logarithmic transformations of the data were used for fitting whenever K^f_i's were separated from K^f_m's by factors exceeding 10.

Acknowledgments

We thank Prof. Katsube for providing PUC119 and Prof. G. Kohlaw for providing 2R,3S-isopropylmalate. Prof. Ken Neet provided much needed advice, support, and encouragement. This work was supported by U.S. Public Health Service grant 1R01 GM48735-01A1 from the National Institutes of Health to A.M.D.

References

Brand L, Witholt B. 1967. Fluorescence measurements. *Methods Enzymol 11*:776-856.

Cleland WW. 1963. The kinetics of enzyme-catalyzed reactions with two or more substrates or products. *Biochim Biophys Acta 67*:188-196.

Dean AM, Koshland DE Jr. 1990. Electrostatic and steric contributions to regulation at the active site of isocitrate dehydrogenase. *Science 249*: 1044-1046.

Dean AM, Koshland DE Jr. 1993. The kinetic mechanism of *Escherichia coli* isocitrate dehydrogenase. *Biochemistry 32*:9302-9309.

Dean AM, Lee MHI, Koshland DE Jr. 1989. Phosphorylation inactivates *Escherichia coli* isocitrate dehydrogenase by preventing isocitrate binding. *J Biol Chem 264*:20482-20486.

Erhlich RS, Colman RF. 1987. Ionization of isocitrate bound to pig heart $NADP^+$-dependent isocitrate dehydrogenase. ^{13}C NMR study of substrate binding. *Biochemistry 26*:2461-2471.

Grissom CB, Cleland WW. 1988. Isotope effect studies of the chemical mechanism of pig heart NADP isocitrate dehydrogenase. *Biochemistry 27*: 2934-2943.

Han S, Pirrung M. 1994. Squarate inhibitors of 3-isopropylmalate dehydrogenase. *J Org Chem 59*:2423-2429.

Head EJH. 1980. NADP-dependent isocitrate dehydrogenase from the mussel *Mytilus edulis* L. *Eur J Biochem 111*:581-586.

Huang CY. 1979. Use of alternative substrates to probe multisubstrate enzyme mechanisms. *Methods Enzymol 63*:486-500.

Hurley JH, Dean AM. 1994. Structure of 3-isopropylmalate dehydrogenase in complex with NAD^+: Ligand-induced loop closing and mechanism for cofactor specificity. *Structure 2*:1007–1016.

Hurley JH, Dean AM, Koshland DE Jr, Stroud RM. 1991. Catalytic mechanism of $NADP^+$-dependent isocitrate dehydrogenase: Implications from the structures of magnesium-isocitrate and $NADP^+$ complexes. *Biochemistry 30*:8671–8678.

Hurley JH, Dean AM, Stohl JL, Koshland DE Jr, Stroud RM. 1990. Regulation of an enzyme by phosphorylation at the active site. *Science 249*: 1012–1016.

Hurley JH, Thorsness P, Ramalingham V, Helmers N, Koshland DE Jr, Stroud RM. 1989. Structure of a bacterial enzyme regulated by phosphorylation, isocitrate dehydrogenase. *Proc Natl Acad Sci USA 86*:8635–8639.

Imada K, Sato M, Tanaka N, Katsube Y, Matsuura Y, Oshima T. 1991. Three-dimensional structure of a highly thermostable enzyme, 3-isopropylmalate dehydrogenase of *Thermus thermophilus* at 2.2 Å resolution. *J Mol Biol 222*:725–738.

Kagawa Y, Nojima H, Nukiwa N, Ishizuka M, Nakajima T, Yasuhara T, Tanaka T, Oshima T. 1984. High guanine plus cytosine content in the third letter of codons of an extreme thermophile: DNA sequence of the 3-isopropylmalate dehydrogenase of *Thermus thermophilus*. *J Biol Chem 259*:2956–2960.

Kakinuma K, Ozawa K, Fujimoto Y, Akutsu N, Oshima T. 1989. Stereochemistry of the decarboxylation reaction catalyzed by 3-isopropylmalate dehydrogenase from thermophilic bacterium *Thermus thermophilus*. *J Chem Soc Chem Commun 232*:1190–1192.

Kunkel TA. 1985. Rapid and efficient site-specific mutagenesis without phenotypic selection. *Proc Natl Acad Sci USA 82*:488–492.

Lienhard GE, Rose IA. 1964. The stereospecific protonation of the enolate form of α-ketoglutarate bound to isocitrate dehydrogenase. *Biochemistry 3*:185–189.

Londesborough JC, Dalziel K. 1968. The mechanisms of reductive carboxylation reactions. *Biochem J 110*:223–230.

Londesborough JC, Dalziel K. 1970. Kinetic studies of NADP-dependent isocitrate dehydrogenase. In: Sund H, ed. *Pyridine nucleotide dependent dehydrogenases*. Berlin: Springer-Verlag. pp 315–323.

Miyazaki K, Kakinuma K, Terasawa H, Oshima T. 1993. Kinetic analysis on the substrate specificity of 3-isopropylmalate dehydrogenase. *FEBS Lett 332*:35–36.

Northrop DB, Cleland WW. 1974. The kinetics of pig heart triphosphopyridine nucleotide-isocitrate dehydrogenase. *J Biol Chem 249*:2928–2931.

Sambrook J, Fritsch EF, Maniatis T. 1989. *Molecular cloning, 2nd ed.* Cold Spring Harbor, New York: Cold Spring Harbor Laboratory Press.

Sanger F, Nicklen S, Coulsen AR. 1977. DNA sequencing with chain terminating inhibitors. *Proc Natl Acad Sci USA 74*:5463–5467.

Siebert G, Carsiotis M, Plaut GWE. 1957. The enzymatic properties of isocitric dehydrogenase. *J Biol Chem 226*:977–991.

Steinberger R, Westheimer FH. 1951. β-Decarboxylation of α-keto acids as catalyzed by divalent metal cations. *J Am Chem Soc 73*:429–435.

Tipton PA, Beecher BS. 1994. Tartrate dehydrogenase, a new member of the family of metal-dependent decarboxylating R-hydroxyacid dehydrogenases. *Arch Biochem Biophys 313*:15–21.

Tipton PA, Peisach J. 1991. Pulsed EPR analysis of tartrate dehydrogenase active-site complexes. *Biochemistry 29*:1749–1756.

Uhr ML, Thompson VW, Cleland WW. 1974. The kinetics of pig heart triphosphopyridine nucleotide-isocitrate dehydrogenase. *J Biol Chem 249*:2920–2927.

Yamada T, Akutsu N, Miyazaki K, Kakinuma K, Yoshida M, Oshima T. 1990. Purification, catalytic properties, and thermal stability of *threo*-D_s-3-isopropylmalate dehydrogenase coded by *LeuB* gene from extreme thermophile, *Thermus thermophilus* strain HB8. *J Biochem 108*:449–456.